COBEM 2021 Florianópolis - Brasil
ABCM Associação Brasileira de Engenharia e Ciências Mecânicas
26th ABCM International Congress of Mechanical Engineering
November 22-26, 2021. Florianópolis, SC, Brazil

# COB-2021- 0834
# NUMERICAL STUDY OF SHOCK WAVE REFLECTION WHEN INTERACTING WITH A RIGID WEDGE
# 26th COBEM

**Rodrigo Savi Justi**
Universidade Federal do Rio Grande do Sul, Rua Sarmento Leite, 425
rodrigo.justi@ufrgs.br
**Andrés Armando Mendiburu Zevallos**
Universidade Federal do Rio Grande do Sul, Rua Sarmento Leite, 425
International Research Group for Energy Sustainability (IRGES)
andresmendiburu@ufrgs.br

***Abstract.*** *The reflection of shock waves can be separated into regular reflection (RR) and irregular reflections (IR), the last comprehending Mach Reflections (MR) and von Neumann Reflections (vNR). In unsteady and pseudo-unsteady flow, the MR can be subdivided into simple Mach Reflection (SMR), transitional Mach Reflection (TMR) and double Mach Reflection (DMR). When a plane shock wave hits a wedge, occurs a reflection-diffraction process and then a self-similar reflected shock moves outward while the original shock moves forward in time. The experimental and computational analysis shows that various patterns of reflections can occur, including regular and Mach reflections. The RR-MR transition in planar shock waves with rigid wedge interaction has been an area of much research in past decades and can be studied with both analytical methods and numerical simulations. In a numerical approach, the determination of the boundary between the regular and Mach reflections can be obtained by post-processing of solutions of time-dependent Euler equations in two dimensions for many flow conditions. The objective of this work is to determine numerically this boundary and compare it to experimental data and to the boundary predicted by two- shock and three-shock analytical theories. The solution of Euler equations was performed by fifth order WENO reconstruction finite volume scheme and the fluxes were obtained by HLLC approximated Riemann solver. The time discretization is realized by a TVD third order Rugen-Kutta scheme and the time step was determined by CFL condition. The numerical boundary obtained have a good agreement with the detachment boundary for low Mach numbers ranging from 1.0 to 1.7 but not to the high Mach number ranging from 1.7 to 4.0, as was expected based in another research works in the literature.*

***Keywords:*** *Shock waves, Mach reflection, Euler equations, Riemann solver, WENO reconstruction.*

## 1. INTRODUCTION

When a moving shock wave interacts with a rigid inclined wedge, a formation of different types of reflection patterns can occur. According to Ben Dur (shock waves handbook), the shock waves reflections can be separated into regular reflections (RR), that consists in an incident and in a reflected shock wave and into irregular reflections (IR), that comprehends all of the other wave reflection configurations. The IR can be separated in Mach reflections (MR) and von Neumann reflections (vNR). The Mach reflections involves one slipstream and three shock waves, the incident, the reflected and the Mach stem. The Mach – stem shock extends from the meeting point of the incident and reflected shock wave to the wedge surface. Since other wave patterns have been found in pseudo-steady shock reflection, in steady shock reflection only RR and single-Mach reflection have been observed. This occurs because the pseudo-steady shock reflection is constituted by two subprocesses, shock reflection and shock-induced flow deflection (Li & Ben-Dor 1995). The study of unsteady shock reflection is more complicated and can be found in Bazhenova et a. (1984).

The Mach reflection was first observed by Ernest Mach in 1878 and posteriorly investigated by Smith (1945) and White (1951), who identified from shock tube experiments that the Mach reflection can be subdivided in three types, the single Mach reflection (SMR), double Mach reflection (DMR) and transitional Mach reflection (TMR). Furthermore, the Mach reflection were divided into more specific wave configurations, for more details see Ben-Dor (2007) and Semenov et al. (2012). The analytical approach to describe regular reflection and Mach reflection uses the conservation equations over oblique shock waves and are called two-shock theory and three-shock theory, respectively. Both theories started with von Neumann (1943a, 1943b) in his important research of the reflection phenomena and implies the existence of a contact discontinuity that separates flows of different velocities and densities.

The transition between regular and Mach reflections constitutes a very important object of study in the shock reflection field and have various applications in engineering. The type of reflection pattern depends on the inclination of the wedge,

the gas proprieties, the Mach number of shock wave and initial and boundary conditions. Since White (1945) and Smith (1951), a lot of experimental and numerical research was performed for different conditions and gases. Henderson and Lozzi (1975) provided detailed experimental data on the transition between RR-MR for steady, pseudo-steady and unsteady flows. An experimental investigation of reflection of a planar shock wave over a two-facet concave wedge was carried on by Ginzburg and Markov (1975) and by Srivastava and Deschambault (1984).

Ben-Dor and Glass (1979, 1980) performed experimental and theoretical research on different types of shock reflection within hypervelocity shock tubes in argon, helium and nitrogen, they determined the RR-MR transition boundaries between these gases. Ben-Dor *et al.* (1987) provided a study of a planar shock reflection over a plane double wedge and several complicated wave configurations were also considered. Barbosa and Skews (2002) provides experimental data to the transition boundary between regular and Mach reflection. They built a large shock tube with a channel that first bifurcates into two equal-sized diverging ducts, which slowly bend back together, and finally rejoin.

An experimentally and numerically analysis of shock wave reflections from wedges with straight and concave tips in pseudo-steady flows was realized by Previtali et al. (2015). The numerical simulations use a locally adaptative unstructured Godunov-type second-order TVD finite-volume flow solver, to solve the Euler equations of an ideal gas with constant specific heats. Hryniewicki1 *et al*. (2017) determined the transition boundary between regular and Mach reflections for a moving shock interacting with a wedge in inviscid and polytropic air. The transition boundary numerically determined by the authors is show to agree with the von Neumann's closely spaced sonic and extreme-angle boundaries for weak shocks, that for shock Mach numbers ranging from 1.0 to 1.6, but this limit deviates upward and above for Mach numbers from 1.6 to 4.0. Hryniewicki1*et al*. (2019) also determined numerically the transition boundary between regular and Mach reflections for a moving shock interacting with a wedge in inviscid and polytropic argon and the results agree with von Neumann's closely spaced sonic and extreme-angle boundaries for weak shock, with Mach numbers from 1.0 to 1.55 and deviates upward and above from Mach numbers from 1.55 to 4.0.

In this work, the numerical determination of transition boundary for inviscid air is realized to Mach numbers ranging from 1.0 to 4.0. A FORTRAN 90 code was developed to perform the simulations solving the two-dimensional Euler equations with a fifth order WENO reconstruction finite volume scheme. The numerical fluxes were evaluated by HLLC approximated Riemann solver and the time update solution was performed by TVD third order Rugen-Kutta scheme.

## 2. TRANSITION CRITERION FOR REFLECTION

Shock waves are finite amplitude mechanical waves that arise when the matter is subject to fast compression. When the shock wave is perpendicular to the flow it is called normal shock wave. The normal shock waves can be analyzed in either of two reference frames, in standing normal shock and in movement shock. The flow behind a normal shock wave must be supersonic and the flow ahead a normal shock must be subsonic. The strength of a incident shock is specified by his Mach number, that is the velocity $V_i$ divided by the sound speed $a_1$, that is:

$$M_i = \frac{V_i}{a_1} \tag{1}$$

The gas properties immediately before and after being shocked are related by the Rankine-Hugoniot jump conditions. Using these conditions, it is possible to determine the density and pressure in terms of shock Mach number, as expressed in Equations (2) and (3). The $\rho_1$ and $\rho_2$ are the densities before and after shock, respectively, and $p_1$ and $p_2$ the pressure before and after shock, respectively, and $\gamma$ is the adiabatic index.

$$\frac{\rho_2}{\rho_1} = \frac{(\gamma+1)M_i^2}{(\gamma-1)M_i^2+2} \tag{2}$$

$$\frac{p_2}{p_1} = \frac{2\gamma M_i^2 - (\gamma-1)}{\gamma+1} \tag{3}$$

The regular reflections occur typically at larger wedge angles, while single-Mach reflections occur typically at smaller wedge angles. Double and transitional-Mach reflections occur for mid to low wedge angles and for large incident shock Mach numbers (Hryniewicki1 *et al.*, 2019). The transition criterion between regular reflections (RR) and irregular reflections (IR) has been subject of several studies since von Neumann's first studies in 1940s. There are three types of flow that can be pointed out studying shock reflection: the steady flow, pseudo-steady flow and unsteady flow. The pseudo-steady flow can be led to a steady flow by appropriate transformation coordinates and is possible to introduce self-similar variables, because there is no characteristic length (Shtemenko and Shugaev, 1998). The reflection of a plane shock from an infinite wedge is a pseudo-steady flow. The boundary transition can be determined analytically by the mechanical equilibrium criteria and detachment criteria. There are three regions determined by these two boundaries: an upper region (Region 1) only for regular reflection, a dual region (Region 2) for either regular reflection or Mach reflection

between the two boundaries, and a lower region (Region 3) for only Mach reflection (SMR, TMR, and DMR). These regions and boundaries will be shown in Figure (5) in the Results and Discussion.

The establishment of the detachment criterion between regular and Mach reflections was proposed by von Neumann (1943a, 1943b, 1945) assuming ideal gas behavior and that the flow was inviscid. This criterion is based on the two-shock theory and the detachment boundary. In terms of wedge angle θ and the Mach $M_1$ number the following expressions can be written.

$$a = \frac{1+(\gamma-1)d}{3}, \qquad b = 2d - d^2, \qquad c = \gamma d^2$$
$$d = \frac{2}{(\gamma+1)}\frac{M_i^2-1}{M_i^2}, \qquad e = \sqrt{a^2+b/3}, \qquad f = \cos^{-1}\left(\frac{ab+2a^3-c}{2e^3}\right) \tag{4}$$

$$\cos(\theta) = \frac{1}{a+2\,e\,cos(f/3)} \tag{5}$$

Then, the detachment criterion is represented by the red curve found in Figure 6. The mechanical equilibrium criterion was established based on the three-shock theory and was also proposed by von Neumann (1943a). The relation between the wedge angle and the Mach number is shown in Equations (6) and (7).

$$a = 4d + 2(\gamma-1)(\gamma+2)d^2 - (\gamma^2-1)d^3, \quad b = \gamma + 3 - 1/2\,(5-\gamma)(\gamma+1)d + 2\gamma\,d^2$$
$$c = 4 - 4d, \qquad d = \frac{2}{(\gamma+1)}\frac{M_i^2-1}{M_i^2}, \tag{6}$$

$$\cos^2\theta = \frac{c}{b+\sqrt{b^2-ac}} \tag{7}$$

Then, by using the above expression the blue curve shown in Figure 6 is obtained. For more information about the reflection transition criterions see Henderson (1987).

## 3. NUMERICAL SOLUTION

The numerical solutions were performed by a FORTRAN 90 code developed by the authors. The physical method adopted was the two-dimensional Euler equations with the ideal gas state equation and its solution were performed with a fifth order WENO finite volume scheme, with the numerical fluxes computed by the HLLC approximated Riemann solver. The code generates a uniform cartesian mesh and the basic operation is schematized in the Figure 1. The detailed processes are presented in the next sections.

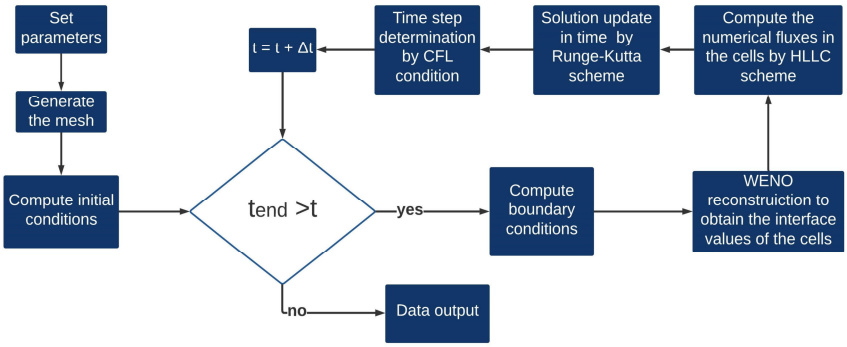


Figure 1. Schematization of code operation.

### 3.1 Gas dynamics equations

According to Toro (2013), the time-dependent Euler equations consist in a system of non-linear hyperbolic conservation laws that describes the dynamical behavior of compressible materials, such as gases, for which the body forces, heat and viscous effects can be neglected. In two dimensions, these equations can be written in the conservative form shown in Eq. (8).

$$\boldsymbol{u}_t + \boldsymbol{f}(\boldsymbol{u})_x + \boldsymbol{g}(\boldsymbol{u})_y = \boldsymbol{0} \tag{8}$$

The vector $\boldsymbol{u}$ represents the conservative variables and the vectors $\boldsymbol{f}(\boldsymbol{u})$ and $\boldsymbol{g}(\boldsymbol{u})$ represent the fluxes,

$$\boldsymbol{u} = \begin{bmatrix} \rho \\ \rho u \\ \rho v \\ E \end{bmatrix}, \quad \boldsymbol{f} = \begin{bmatrix} \rho u \\ \rho u^2 + p \\ \rho uv \\ u(E+p) \end{bmatrix}, \quad \boldsymbol{g} = \begin{bmatrix} \rho v \\ \rho uv \\ \rho v^2 + p \\ v(E+p) \end{bmatrix} \tag{9}$$

where $u$ is the velocity component in the $x$ direction, $v$ is the velocity component in $y$ direction, $\rho$ is the density, $E$ is the total energy and $p$ is the pressure. The total energy is determined by Eq. (10) and the equation of state is the ideal gas equation.

$$E = \frac{p}{\gamma - 1} + \frac{\rho(u^2 + v^2)}{2} \tag{10}$$

Physically, the Euler equations result naturally from the application of the laws of conservation of mass, momentum and energy. In the next section the finite volume method will be addressed.

### 3.2 Finite Volume Method

The code developed uses the finite volume method (FVM) to solve Euler equations. The finite volume methods are widely used to solve fluid dynamics problems and comparing to the standard finite difference methods, that can be expected to break down near discontinuities, the Finite volume methods admits discontinuous solutions thanks to the integral formulation (LeVeque, 2002). The basic idea behind the finite volume method consists in subdividing the domain in a mesh composed by cells or control volumes, at which the solution is represented by the cell average of the conserved quantity.

Consider the uniform discretization of the domain $[x_L, x_R] \times [y_L, y_R]$. The central points are defined as $x_{i,j} = x_L + (i + 1/2)\Delta x$ for $i = 0, \dots, N$ and $y_{i,j} = y_L + (j + 1/2)\Delta y$ for $j = 0, \dots, M$, where $\Delta x = (x_R - x_L)/(N + 1)$ and $\Delta y = (y_R - y_L)/(M + 1)$. The midpoint values are $x_{i-1/2,j} = x_{i,j} - \Delta x/2$ for $i = 0, \dots, N + 1$ and $y_{i,j-1/2} = y_{i,j} - \Delta y/2$ for $j = 0, \dots, M + 1$. The time-step is defined as $\Delta t$ and the time level as $t^n = n\Delta t$. From that, the computational cells are defined as $\mathsf{C}_{ij} = [x_{i-1/2,j}, x_{i+1/2,j}] \times [y_{i,j-1/2}, y_{i,j+1/2}]$. Integrating the Euler relation in conservative form, Equations (9), over the cell $\mathsf{C}_{ij}$, the semi-discrete form, shown in Equation (11), is obtained.

$$\frac{d\boldsymbol{u}_{i,j}}{dt} = \frac{(\boldsymbol{f}_{i-1/2,j} - \boldsymbol{f}_{i+1/2,j})}{\Delta x} + \frac{(\boldsymbol{g}_{i,j-1/2} - \boldsymbol{g}_{i,j+1/2})}{\Delta y} \tag{11}$$

where $\boldsymbol{u}_{i,j}$ is the spatial average of $\boldsymbol{u}$ in the cell $\mathsf{C}_{ij}$ at time $t$

$$\boldsymbol{u}_{i,j} = \frac{1}{\Delta x \Delta y} \int_{y_{i,j-1/2}}^{y_{i,j+1/2}} \int_{x_{i-1/2,j}}^{x_{i+1/2,j}} \boldsymbol{u}(x, y) dx dy \tag{12}$$

and the $\boldsymbol{f}_{i+1/2,j}$ and $\boldsymbol{g}_{i,j+1/2}$ are the spatial averages of physical fluxes in $(x_{i+1/2,j}, y_{i,j})$ and $(x_{i,j}, y_{i,j+1/2})$ of the cells, respectively, at time $t$.

### 3.3 WENO reconstruction

To improve the high-order spatial accuracy, a fifth order WENO reconstruction scheme was used. The WENO schemes were originally proposed by Liu et al (1994) and have been improved by Jiang and Shu (1996). These schemes are based on the successful ENO schemes (Harten et al., 1987; Shu and Osher, 1988, 1989). The main advantage of the WENO schemes is the high accuracy obtained in smooth regions while keeping stable, non-oscillatory and sharp discontinuity transitions (Shu, 2009). The basic idea of WENO schemes is constructing a weighted combination of many local reconstructions with different stencils and use them to find a final approximation.

For simplicity, consider a uniform mesh in one dimension and that it is desired to approximate de function $\boldsymbol{u}(x, y)$ at the half nodes $x_{i+1/2,j}$ and $x_{i-1/2,j}$. The main idea is to find a final fifth order approximation along the stencil $S = \{x_{i-2,j}, x_{i-1,j}, x_{i,j}, x_{i+1,j}, x_{i+2,j}\}$ as a convex combination of third order approximations $\boldsymbol{u}^{(1)}_{i+1/2,j}$, $\boldsymbol{u}^{(2)}_{i+1/2,j}$ and $\boldsymbol{u}^{(3)}_{i+1/2,j}$ to

$\boldsymbol{u}_{i+1/2,j}$ and $\boldsymbol{u}^{(1)}_{i-1/2,j}$, $\boldsymbol{u}^{(2)}_{i-1/2,j}$ and $\boldsymbol{u}^{(3)}_{i-1/2,j}$ to $\boldsymbol{u}_{i-1/2,j}$. The WENO reconstruction leads to the approximations of the type shown in Equation (13), where $\omega_k$ for $k = 1, 2, 3$ are the positive weights with $\omega_1 + \omega_2 + \omega_3 = 1$.

$$\boldsymbol{u}_{i+1/2,j} = \sum_{k=1}^{3} \omega_k \boldsymbol{u}^{(k)}_{i+1/2,j} \tag{13}$$

In the finite volume method, we use the WENO approximation to obtain the value $\boldsymbol{u}_{i+1/2,j}$. A complication of this procedure is the upwinding, where solution to the conservation law, Equation (9), follows characteristics, hence a stable numerical scheme should also propagate its information in the same characteristic direction (Shu, 2009). Then, we replace the numerical flux $\boldsymbol{f}_{i+1/2}$ by the expression given below.

$$\boldsymbol{f}_{i+1/2} = \boldsymbol{f}(x^{-}_{i+1/2,j}, x^{+}_{i+1/2,j}) \tag{14}$$

where $\boldsymbol{f}(x^{-}_{i+1/2,j}, x^{+}_{i+1/2,j})$ is a monotone numerical scheme that is consistent with the physical fluxes. The values of $\boldsymbol{u}^{-}_{i+1/2,j}$ and $\boldsymbol{u}^{+}_{i+1/2,j}$ are the WENO reconstructions from stencils one point biased to the left and one point biased to the right, respectively. The fifth order WENO reconstruction to $\boldsymbol{u}^{-}_{i+1/2,j}$ uses the stencil $x_{i-2,j}$, $x_{i-1,j}$, $x_{i,j}$, $x_{i+1,j}$ and $x_{i+2,j}$ and to $\boldsymbol{u}^{+}_{i+1/2,j}$ the stencil $x_{i-1,j}$, $x_{i,j}$, $x_{i+1,j}$, $x_{i+2,j}$ and $x_{i+3,j}$.

In cartesian meshes, the two-dimensional WENO reconstruction can be easily obtained with the dimension-by-dimension method with the unidimensional procedure to each dimension. For more information about WENO procedure see Jiang and Wu (1999) and Shu (2009). The ENO/WENO schemes to systems of conservation laws have many ways to generalize. In this work, is used the characteristic decomposition, which is more robust, but more computationally intensive, than other simpler implementations (Jiang and Wu, 1999).

### 3.4 Numerical fluxes

In this work, the numerical fluxes were calculated by the HLLC approximated Riemann solver. The solutions of local Riemann problems constitute a modern class of shocking capturing methods for computational fluid dynamics. These techniques based in Riemann problem are known as Godunov methods. Consider the Riemann problem to unidimensional time-dependent Euler equations to a perfect gas with the following initial conditions:

$$\begin{aligned} &\boldsymbol{u}_t + \boldsymbol{f}(\boldsymbol{u})_x = \boldsymbol{0} \\ &\boldsymbol{u}(x, \boldsymbol{0}) = \begin{cases} \boldsymbol{u}_L, & x < 0 \\ \boldsymbol{u}_R, & x > 0 \end{cases} \end{aligned} \tag{15}$$

The structure of the solution has three waves and looks like shown in Fig (2). The right and left waves can be either rarefactions or shocks and are called non-linear waves, while the middle wave is always a contact discontinuity. The contacts and shocks are discontinuities solutions and rarefactions are continuous solutions. There are four possible patterns to the waves. The region between left and right waves are called the star region and have constant pressure, $p^*$, and constant velocity, $u^*$, while the density changes discontinuously across the contact to $\rho_L^*$ from the left and to $\rho_R^*$ from the right.

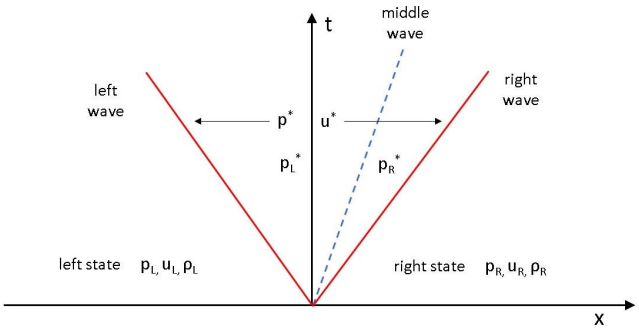


Figure 2. Structure of the Riemann problem solution.

The approximated Riemann solver HLL proposed by Harten Lax and van Leer (1983) requires the estimative for the fastest signal velocities emerging from the initial discontinuity at the interface, resulting in a two–wave model for the structure of the exact solution (Toro, 2013). A more accurate three-wave model called HLLC was proposed by Toro et

al. (1992) and results in better resolution of intermediate waves. To compute the numerical flux $\boldsymbol{f}_{i+1/2,j}$ in a cell $C_{i,j}$, the left state of conservative variables $\boldsymbol{u}_L$ corresponds to $\boldsymbol{u}^-_{i+1/2,j}$ and the right state of conservative variables $\boldsymbol{u}_R$ corresponds to $\boldsymbol{u}^+_{i+1/2,j}$ obtained in WENO reconstruction. The same procedure is used to compute the numerical flux $\boldsymbol{g}_{i,j+1/2}$.

### 3.5 Time discretization

There a several methods to solve ordinary differential equations and a class of explicit scheme widely used for conservation laws is called explicit Runge-Kutta methods. The finite volume scheme expressed in Eq (11) can be written as a method-of-lines ordinary differential equations system:

$$\frac{d\boldsymbol{u}_{i,j}}{dt} = \boldsymbol{L}(\boldsymbol{u})_{i,j} \tag{16}$$

This system can be discretized by the total variation diminishing (TVD) Runge–Kutta methods, also known as the method of strong stability preserving (SSP). These methods were first developed by Shu and Osher (1988) and Shu (1988). In the present work, a third order TVD Runge-Kutta method (SSPRK3) was used to obtain the solution update in time and the solution consists in following steps:

$$\boldsymbol{u}^{(1)} = \boldsymbol{u}^n + \Delta t L(\boldsymbol{u}^n) \tag{17}$$

$$\boldsymbol{u}^{(2)} = \frac{3}{4}\boldsymbol{u}^n + \frac{1}{4}\boldsymbol{u}^{(1)} + \frac{1}{4}\Delta t L(\boldsymbol{u}^n) \tag{18}$$

$$\boldsymbol{u}^{n+1} = \frac{1}{3}\boldsymbol{u}^n + \frac{2}{3}\boldsymbol{u}^{(2)} + \frac{2}{3}\Delta t L(\boldsymbol{u}^{(2)}) \tag{19}$$

The time step was determined by the Courant–Friedrichs–Lewy condition expressed in Equation (20).

$$\Delta t = min\ CFL\left(\frac{\Delta x}{S^n_{x,max}}, \frac{\Delta y}{S^n_{y,max}}\right), \qquad \begin{aligned} S^n_{x,max} &= \max_{i,j}\{|u^n_{i,j}| + a^n_{i,j}\} \\ S^n_{y,max} &= \max_{i,j}\{|u^n_{i,j}| + a^n_{i,j}\} \end{aligned} \tag{20}$$

### 3.6 Boundary and initial conditions and code validation

In the wedge, the reflective boundary conditions were used. However, in the rest of the domain frontiers the transmissive boundary conditions were used. The conditions behind the shock were determined by the Equations (2) and (3). The code was validated simulating a test described by Stone *et al.* (2008), with Mach 10 shock set up, with initial position $x = 1/6$ on the lower boundary and whose propagation direction is in the x-axis. The domain is $x = [0, 3.25]$ and $y = [0,1]$, with spatial resolutions of $[N_x, N_y] = [520,160]$ grid cells. The adiabatic coefficient was $\gamma = 1.4$ and an undisturbed gas state $[\rho, p, v_x, v_y] = [1.4, 1.0, 0, 0]$ was adopted. The rigid wedge initiates in $x = 1/6$ and the simulation is run until $t = 0.2$ with $CFL = 0.7$. The solution is computed with Roe fluxes and uses a third order spatial reconstruction. The results are showed in Figure 3.

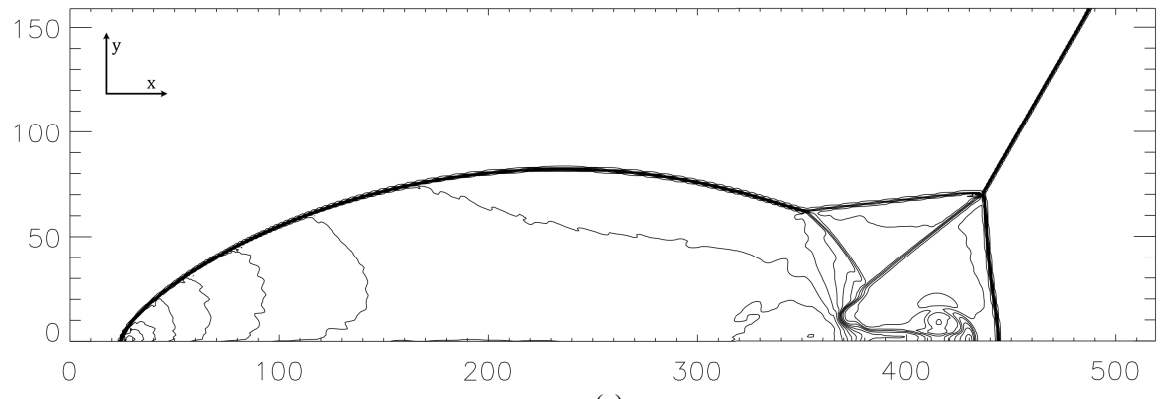


(a)

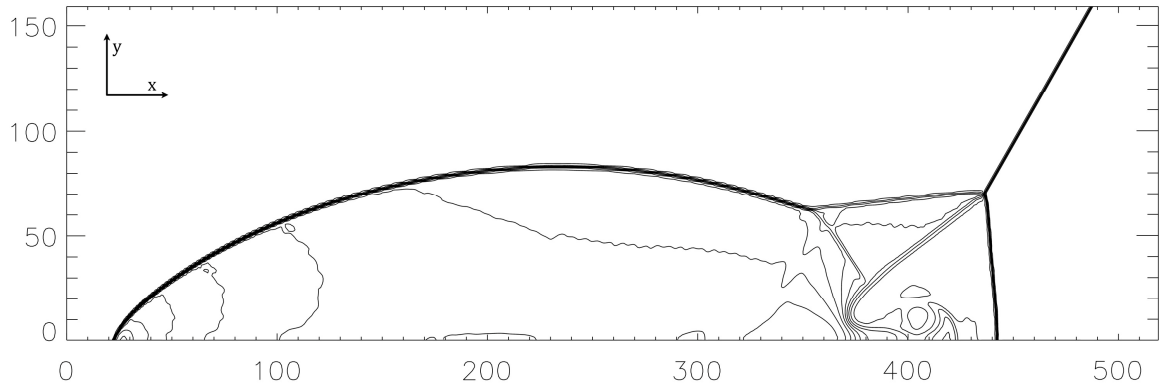


(b)

Figure 3. Density contours for $t = 0.2$ obtained by Stone *et al.* (2008) in (a) and by Justi and Mendiburu (2021) in (b). The two triple shock confluence points indicates that occurs a Double Mach reflection.

## 4. DETERMINATION OF TRANSITION BOUNDARY

The determination of the transition boundary between regular and Mach reflection is based on the data generated by the numerical computations, fixing the Mach number and increasing the wedge angle from a small value, at which occurs a Mach reflection, until the Mach stem disappears and regular reflection starts. The determination of the numerical transition boundary needs a characteristic length $L^*$ of the Mach stem, that was defined as shown in Equation (21).

$$L^* = \frac{L_m - L_i}{L_i} \tag{21}$$

The dimensionless length $L^*$ diminishes to zero as the results get closer to the transition boundary. These lengths are illustrated in Figure 4.

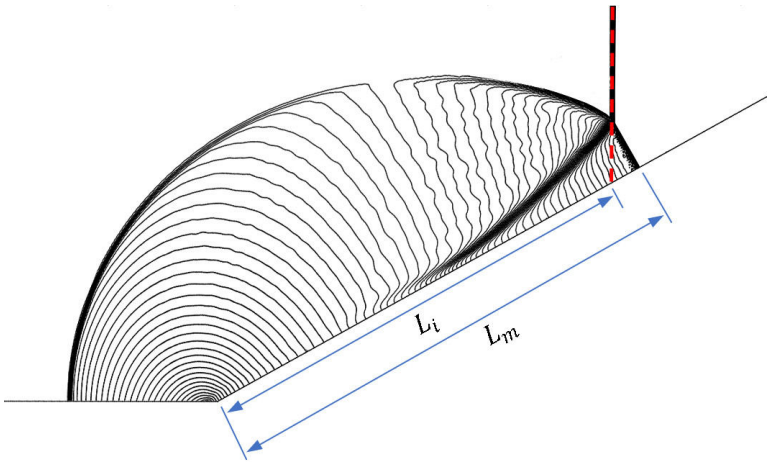


Figure 4 – Velocity contours and indication of lengths $L_m$ and $L_i$ with a $M_i = 1.5$ shock and a wedge angle $\theta = 30°$. The grid has 650x200 cells and the plot 100 contours.

More details about the length $L$ and other lengths of relevance can be found in Nam (2005). To determine the boundary limit numerically, 12 points of reference along the detachment boundary were used. For each of these points it was stablished a wedge angle $\beta$ to start the simulations. With a fixed Mach number, the simulations were realized increasing the angle by 0.5 degree. These reference points and the ranges are showed in Table 1.

Table 1. Reference points and the angle that simulations start.

| $M_i^*$ | 1.01 | 1.05 | 1.10 | 1.15 | 1.25 | 1.45 | 1.70 | 2.0 | 2.50 | 3.00 | 3.50 | 4.00 |
|---|---|---|---|---|---|---|---|---|---|---|---|---|
| $\theta^*(°)$ | 15.47 | 29.92 | 37.07 | 40.95 | 45.11 | 48.52 | 50.00 | 50.59 | 50.77 | 50.70 | 50.60 | 50.51 |
| $\beta(°)$ | 12.00 | 25.00 | 34.00 | 36.00 | 41.00 | 44.00 | 46.00 | 46.00 | 46.00 | 46.00 | 46.00 | 46.00 |

## 5. RESULTS AND DISCUSSION

After the simulations were performed for air, the next step was the post processing of the results. The Mach stem of the data closer to the transition boundary is very small to be determine accurately. Then, only data for well identified Mach stems are included in the curve fit. In Figure 5 (a) it is shown the Mach stem from a simulation realized in this process. It is possible to observe that when the conditions approximate the boundary transition, it becomes difficult to determine $L^*$ precisely. A higher accuracy can be obtained by refining the computational mesh and using higher order schemes. For each Mach number, the characteristic length $L^*$ of all simulations were plotted, and an interpolation polynomial is used to determinate the value of the angle for $L^* = 0$. This method was used to determine three transition boundaries for all Mach numbers. The Figure 6 (b) shows the values of $L^*$, the interpolation curve and the angle of occurrence of the transition.

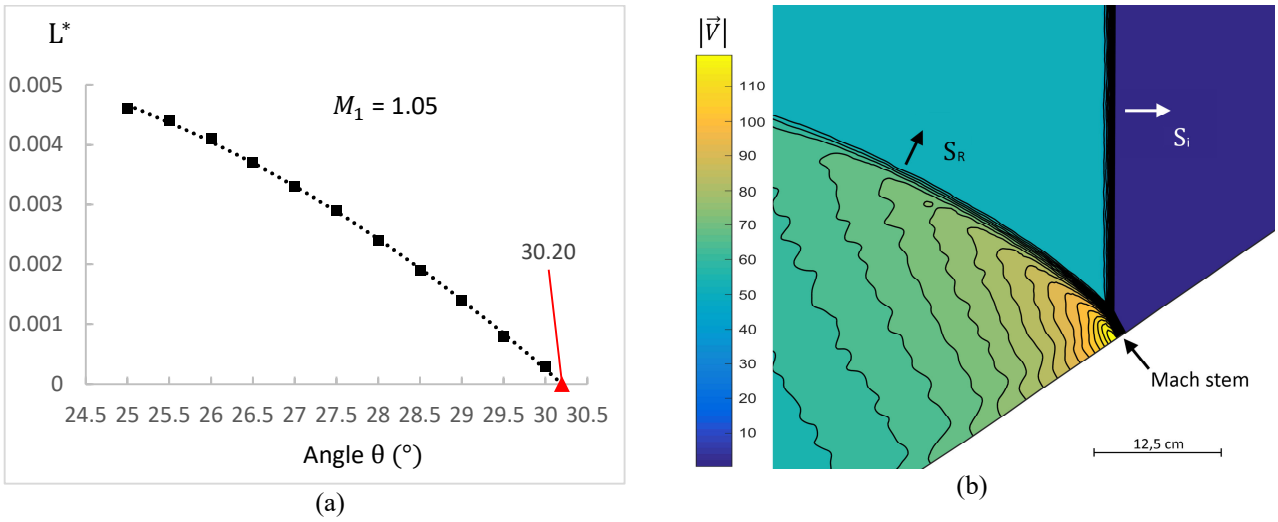


Figure 5 – (a) Interpolation of characteristic length $L^*$ to simulations with $M_1 = 1.05$. The angle correspondent to the boundary limit is determined when trendline cross the axis; (b) Velocity field from a simulation with $M_i = 1.1$ and $\theta = 34.0°$ and 1500x500 grid. In this configuration occurs a SMR, with de characteristic length $L^* = 0.0014$.

In the Figure 5 (b) we can see the incident shock in $S_i$, the reflected shock $S_R$ and the Mach stem formed by the fusion of incident and reflected shock. As we can see, as soon as conditions start to approach into the boundary transition, the determination of $L^*$ becomes difficult. The results were compared with experimental data from Smith (1959), Henderson and Lozzi (1975, 1979), Barbosa and Skews (2002) and Herron and Skews (2011). This data is presented in Table 2. The results obtained for the 12 Mach numbers were compared with the numerical results, the experimental data, the detachment and mechanical equilibrium boundaries are showed in Figure 6. As can be observed, for low Mach numbers ranging from 1.0 to 1.7, the numerical results have a good agreement with the detachment criterion. For Mach numbers higher than 1.7, the numerical boundary tends to be above the detachment boundary, and is located in the dual region, where both regular reflection and Mach reflection can occur.

Table 2. Experimental data from shock tube experiments.

| $M_1$ | $\theta$ | Reference |
|---|---|---|
| 1.0223 | 20.0° | Herron and Skews (2011). |
| 1.039 | 27.5° | Smith (1959) |
| 1.08 | 33.5° | Henderson and Lozzi (1975) |
| 1.13 | 38.8° | Henderson and Lozzi (1979) |
| 1.144 | 40.0° | Barbosa and Skews (2002) |
| 1.3724 | 48.0° | Herron and Skews (2011) |
| 1.88 | 51.0° | Henderson and Lozzi (1975) |

The numerical results for this pseudo-steady flow simulations seems to not agree very well with the mechanical equilibrium boundary. However, according to Hryniewicki1*et al.* (2017), in the case of steady supersonic flows over wedges, the two transition boundaries for MR to RR and RR to MR are known to be more or less close to von Neumann's mechanical-equilibrium and detachment boundaries, respectively. Therefore, that involves the dual region.

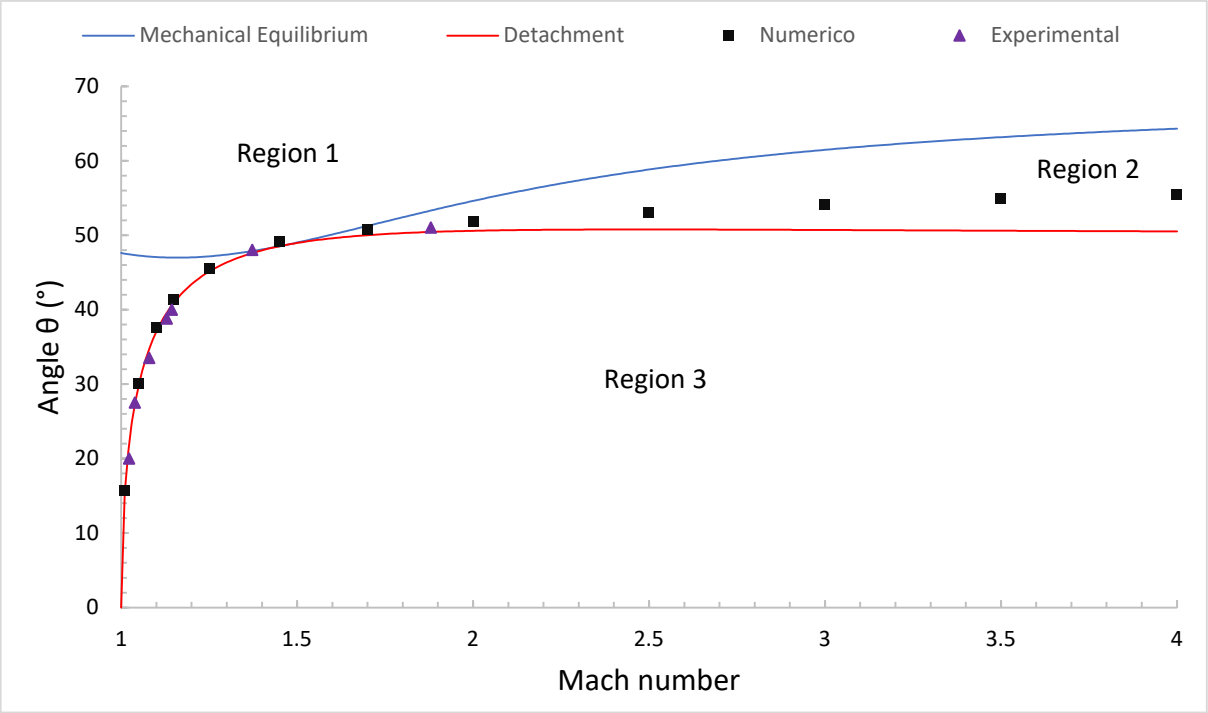


Figure 6. Comparation of numerical results, obtained in the present work, with experimental data and analytical theories. As possible to see the agreement of numerical results with the detachment criterion and experiments for low Mach numbers. When Mach numbers increase, the results are in dual region (Region 2).

## 6. CONCLUSION

In conclusion, the agreement of the results with the analytical theory, experimental data and another works shows that the physical model without boundary layer provides satisfactory results. However, a study solving the Navies Stokes equations is also interesting for evaluation.

An objective of this work was exploring the applications of the WENO reconstruction schemes. The results obtained in this work suggest that the fifth order WENO finite volume scheme associated with the HLLC numerical fluxes can be a good alternative to obtain numerical solutions of problems involving shock waves. This study considered 12 reference points and variated the wedge angle by 0.5 degrees at each simulation. Therefore, a future study could consider a higher number of the reference points and a slighter variation of the wedge angle.

In this work, was not realized a study of mesh refinement on solution accuracy. This kind of study can determine the effects of mesh refinement in the accuracy of flow-field solutions.

Finally, the code can be improved by the implementation of an adaptive mesh refinement (AMR) method to adapting the precision of the numerical computation in specific areas and consequently make the code more efficient.

## 7. REFERENCES

Barbosa, Filipe J., and Beric W. Skews. "Experimental confirmation of the von Neumann theory of shock wave reflection transition." *Journal of Fluid Mechanics 472* (2002): 263.

Bazhenova, T. V., L. G. Gvozdeva, and M. A. Nettleton. "Unsteady interactions of shock waves." *Progress in Aerospace Sciences* 21 (1984): 249-331.

Ben-Dor, G., and I. I. Glass. "Domains and boundaries of non-stationary oblique shock-wave reflexions. 1. Diatomic gas." *Journal of Fluid Mechanics 92.3* (1979): 459-496.

Ben-Dor, G., and I. I. Glass. "Domains and boundaries of non-stationary oblique shock-wave reflexions. 2. Monatomic gas." *Journal of Fluid Mechanics 96.4* (1980): 735-756.

Ben-Dor, G., J. M. Dewey, and K. Takayama. "The reflection of a plane shock wave over a double wedge." *Journal of Fluid Mechanics 176* (1987): 483-520.

Ben-Dor, Gabi, and Gabi Ben-Dor. *Shock wave reflection phenomena*. Vol. 2. New York: Springer, 2007.

Ginzburg, I. P., and Iu S. Markov. "Experimental investigation of the reflection of a shock wave from a two-facet wedge." *Gazodinamika i Teploobmen 4.3* (1975): 74-81.

Gottlieb, J. J., M. K. Hryniewicki, and C. P. T. Groth. "Transition boundary between regular and Mach reflections for a moving shock interacting with a wedge in inviscid and polytropic argon." *Shock Waves 29.6* (2019): 795-816.

Harten, Ami, et al. "Uniformly high order accurate essentially non-oscillatory schemes, III." *Upwind and high-resolution schemes. Springer, Berlin, Heidelberg*, 1987. 218-290.

Harten, Amiram, Peter D. Lax, and Bram van Leer. "On upstream differencing and Godunov-type schemes for hyperbolic conservation laws." *SIAM review* 25.1 (1983): 35-61.

Henderson, L. F. "Regions and boundaries for diffracting shock wave systems." *ZAMM-Journal of Applied Mathematics and Mechanics/Zeitschrift für Angewandte Mathematik und Mechanik 67.2* (1987): 73-86.

Henderson, L. F., and A. Lozzi. "Experiments on transition of Mach reflexion." *Journal of Fluid Mechanics* 68.1 (1975): 139-155.

Henderson, L. F., and A. Lozzi. "Further experiments on transition to Mach reflexion." *Journal of Fluid Mechanics* 94.3 (1979): 541-559.

Herron, T., and B. Skews. "On the persistence of regular reflection." *Shock Waves* 21.6 (2011): 573-578.

Hryniewicki, M. K., J. J. Gottlieb, and C. P. T. Groth. "Transition boundary between regular and Mach reflections for a moving shock interacting with a wedge in inviscid and polytropic air." *Shock Waves 27.4* (2017): 523-550.

Jiang, Guang-Shan, and Cheng-chin Wu. "A high-order WENO finite difference scheme for the equations of ideal magnetohydrodynamics." *Journal of Computational Physics* 150.2 (1999): 561-594.

Jiang, Guang-Shan, and Chi-Wang Shu. "Efficient implementation of weighted ENO schemes." *Journal of computational physics 126.1* (1996): 202-228.

Li, H., and G. Ben-Dor. "Reconsideration of pseudo-steady shock wave reflections and the transition criteria between them." *Shock waves* 5.1-2 (1995): 59-73.

Liu, Xu-Dong, Stanley Osher, and Tony Chan. "Weighted essentially non-oscillatory schemes." *Journal of computational physics 115.1* (1994): 200-212.

Nam, Jee-Whan. *Numerical study of planar shock reflection over wedges*. University of Toronto, 2005.

Previtali FA, Timofeev E, Kleine H (2015). “On unsteady shock wave reflections from wedges with straight and concave tips.” *45th AIAA fluid dynamics conference.* Dallas, United States.

Semenov, A. N., M. K. Berezkina, and I. V. Krassovskaya. "Classification of pseudo-steady shock wave reflection types." *Shock Waves* 22.4 (2012): 307-316.

Shtemenko, L. S., and F. V. Shugaev. “Propagation and reflection of shock waves.” *Vol. 49. World Scientific*, 1998.

Shu, Chi-Wang, and Stanley Osher. "Efficient implementation of essentially non-oscillatory shock-capturing schemes." *Journal of computational physics* 77.2 (1988): 439-471.

Shu, Chi-Wang, and Stanley Osher. "Efficient implementation of essentially non-oscillatory shock-capturing schemes." *Journal of computational physics* 77.2 (1988): 439-471.

Shu, Chi-Wang, and Stanley Osher. "Efficient implementation of essentially non-oscillatory shock-capturing schemes, II." *Upwind and High-Resolution Schemes*. Springer, Berlin, Heidelberg, 1989. 328-374.

Shu, Chi-Wang. "High order weighted essentially nonoscillatory schemes for convection dominated problems." *SIAM review* 51.1 (2009): 82-126.

Shu, Chi-Wang. "Total-variation-diminishing time discretizations." *SIAM Journal on Scientific and Statistical Computing* 9.6 (1988): 1073-1084.

Smith, Lincoln G. "Photographic investigation of the reflection of plane shocks in air." *OSRD Report* (1945).

Smith, Wesley Richard. "Mutual reflection of two shock waves of arbitrary strengths." *The Physics of Fluids* 2.5 (1959): 533-541.

Srivastava, R. S., and R. L. Deschambault. "Pressure distribution behind a nonstationary reflected-diffracted oblique shock wave." *AIAA journal 22.2* (1984): 305-306.

Stone, James M., et al. "Athena: a new code for astrophysical MHD." *The Astrophysical Journal Supplement Series* 178.1 (2008): 137.

Toro, E. F., Spruce, M. and Speares, W. “Restoration of the Contact Surface in the HLL–Riemann Solver.” *Technical Report CoA–9204*, Department of Aerospace Science, Collegue of Aeronautics, Cranfield Institute of Technology, UK, 1992.

Toro, Eleuterio F. “Riemann solvers and numerical methods for fluid dynamics: a practical introduction.” *Springer Science & Business Media*, 2013.

Von Neumann, J. "Refraction, intersection and reflection of shock waves." NAVORD Rep. 203-45 (1945).

Von Neumann, John. "Oblique reflection of shocks." *Bureau of Ordinance, Explosives Research Report* (1943a).

Von Neumann, John. “Theory of shock waves.” *National defense research committee of the office of scientific research and development*, United States, (1943b).

White, Donald R. "A Experimental Survey of the Mach Reflection of Shock Waves." *Ph. D. Thesis* (1951).

## 8. RESPONSIBILITY NOTICE

The author(s) is (are) the only responsible for the printed material included in this paper.